Nanoscale

PAPER

View Article Online
View Journal | View Issue

Cite this: *Nanoscale*, 2025, **17**, 16423

Stability matters: evaluating the long-term performance of AuNP–DNA conjugates in lateral flow assays through varied conjugation methods and storage buffers†

Celia Fuentes-Chust, [a] Claudio Parolo, [b] Andrew Piper [a] and Arben Merkoçi *[a,c]

This study evaluates five distinct conjugation techniques for attaching DNA to gold nanoparticles (AuNPs), focusing on their applicability in lateral flow assays (LFA). The selected methods include three salt-aging techniques, one polyT-adsorption method, and a rapid butanol dehydration (INDEBT) approach. These methods were chosen based on factors such as popularity, protocol duration, and ionic strength. Additionally, the study investigates the storage stability of DNA–AuNP conjugates in four different buffers: 100 mM Tris-$MgCl_2$, 10 mM PBS-$MgCl_2$, PBS, and deionized water. These buffers were selected to evaluate the effects of ionic strength and their compatibility with LFA materials on conjugate stability and performance. Results indicate that salt-aging methods, particularly with water or PBS, maintained LFA functionality up to 21 days. Adsorbed DNA and all samples stored in PBS-$MgCl_2$ were not functional from the start and aggregated over time. INDEBT and Tris-$MgCl_2$ conjugates demonstrated initial functionality but degraded due to butanol residues and aggregation. A complementary analysis using electrophoretic mobility shift assays (EMSAs), UV-Vis spectroscopy, and dynamic light scattering (DLS) provided essential insights into conjugate behavior. These results emphasize the importance of buffer selection and conjugation techniques for optimizing DNA–AuNP conjugates in LFAs, ensuring their reliability and effectiveness in diagnostic applications.

Received 18th December 2024,
Accepted 7th May 2025

DOI: 10.1039/d4nr05328a

rsc.li/nanoscale

Introduction

Gold nanoparticle (AuNP)–DNA conjugates have become essential tools across various scientific and technological fields, ranging from biosensing to drug delivery.[1–7] Faulk and Taylor's pioneering work in 1971, which involved conjugating anti-salmonellae antibodies to AuNPs, marked a significant milestone and laid the foundation for subsequent advancements in the field.[8] In the 1980s, the use of AuNPs in lateral flow assays (LFAs) revolutionized point-of-care (PoC) diagnostics, facilitating rapid and user-friendly tests for a wide range of diseases and conditions.[9–11] The work pioneered by Prof. Mirkin in 1996 introduced the conjugation of thiolated nucleic acids to AuNPs expanding the potential of these nanoparticles, leading to the creation of "spherical nucleic acids" (SNAs) and opening the door to advanced molecular diagnostic tools.[1,12]

At the time of writing, AuNP–DNA conjugates are prepared using various conjugation methods, each with its specific protocol and variations thereof.[13–16] These methods vary in terms of ionic strength, pH adjustments, use of surfactants, preservatives, and duration of the conjugation process.[14,17] The widely known salt-aging (SA) method introduced in 1996 involves the gradual addition of salt to stabilize and facilitate DNA attachment to the negatively charged AuNPs. Other methods, such as pH-altered, butanol-mediated, freezing-assisted, and microwave-assisted conjugation, each have their own advantages and disadvantages which are discussed in detail below.[18–21] While this variety of methods offers flexibility in the functionalization of AuNPs with DNA, it can also cause confusion for researchers trying to choose the most suitable protocol for their specific application.[22–24]

It is crucial to comprehend how different conjugation methods and storage conditions affect the stability and functionality of AuNP–DNA conjugates, especially in the context of

[a]*Nanobioelectronics and Biosensors Group, Institut Català de Nanociència i Nanotecnologia (ICN2). UAB Campus, Bellaterra, Barcelona 08193, Spain. E-mail: arben.merkoci@icn2.cat, andrew.piper@icn2.cat*
[b]*INTERFIBIO Research Group, Departament d'Enginyeria Química, Universitat Rovira i Virgili, Tarragona, 43007, Spain. E-mail: claudio.parolo@gmail.com*
[c]*ICREA, Institució Catalana de Recerca i Estudis Avançats, Pg. Lluís Companys 23, Barcelona 08010, Spain*

† Electronic supplementary information (ESI) available. See DOI: https://doi.org/10.1039/d4nr05328a

LFAs.[25] Stability of AuNPs–DNA conjugates refers to their ability to retain their size, prevent aggregation, and retain their optical properties over time, while functionality pertains to their capability to hybridize with complementary sequences, which is essential for effective biosensing.[18,26] In order to retain functionality it is necessary to guarantee the accessibility of the DNA molecules on the AuNP surface, while at the same time ensure a high enough packing density to prevent the aggregation of the AuNPs themselves.[27]

In this study, we evaluated five different conjugation methods and four different storage buffer solutions to understand their impact on the stability and functionality of the AuNP–DNA conjugates. The selection of five conjugation techniques considered factors such as popularity, protocol duration, conjugation chemistry, number of steps, and ionic strength; with those investigated chosen to be as representative as possible of those widely used in the literature and 1 more modern alternative (butanol assisted).[28] These representative techniques consist of three SA methods, one polyT-adsorption method, and one rapid butanol dehydration method. SA methods are widely utilized for their facilitation of covalent conjugation (Fig. 1). Specifically, we chose three different SA methods to encompass a variety of parameters including pH, time, and ionic strength. In all these methods thiolated DNA was used so covalent Au–thiolate bonds are formed. In thiolate self-assembled monolayer formation, there is a rapid stochastic binding of the thiolates to the Au followed by a rearrangement to a thermodynamically stable steady state.[28] In the AuNP–DNA system the negative charge of the citrate repels the anionic phosphate backbone of the DNA which electrostatically inhibits binding, this can be overcome by adding salt in the SA process.[29–31] As well as shielding the Au-citrate from the DNA, the salt addition shields neighbouring DNA molecules on the surface of the nanoparticles, allowing for higher packing densities. The first SA method, originally reported by Mirkin *et al.* and Alivisatos *et al.*, relies on the gradual addition of 1 M NaCl and 0.1 M sodium phosphate buffer, at pH 7, and takes 3 days to complete.[30,32] However, in our experimental setup, increasing the NaCl concentration beyond 0.1 M consistently led to nanoparticle aggregation, which hindered the formation of stable DNA–AuNP conjugates. To address this, we optimized the protocol to prevent aggregation while maintaining functionalization efficiency. We attribute this change in tolerance to increasing salt concentrations to our use of a more hydrophobic C6 thiol linker than the PEG thiol linker used by Alvisatos *et al.* Whilst more modern versions of this protocol have been developed and published, this original protocol is still widely used so was deemed worthy of investigation. The second method, a pH-altered SA protocol (SA-pH), involves pH adjustments to 5.2 and 8.2 to enhance conjugation efficiency, reducing the protocol duration to two days.[33] The third method, optimized for LFAs (SA-LFA), incorporates surfactants and sonication to prevent aggregation and improve flow properties, also takes two days. The polyT-adsorption method relies on electrostatic interactions between DNA nucleobases and citrate anions on the gold surface (Fig. 1, left).[34] We would like to clarify that the oligonucleotides used in our study contain thiol groups, which covalently bind to the gold nanoparticles. While adsorption methods often involve poly-A or poly-T sequences or positively charged polymers like PEI, our protocol employed a poly-T(14) sequence for to further bind the DNA to the nanoparticles through physisorption of this 14-T linker. Although in the literature this is often referred to as non-covalent binding it should be reiterated that there is a covalent attachment of the thiol to the Au, and so there is chemisorption as well as the physisorption. These interactions are present in all of the conjugations tested, but this method of conjugation by these forces alone is still commonly used in the literature and serves as a useful control for the other conjugation protocols in the experiments herein. No changes in the buffer were used for this method. This method is widely used, it can be completed in approximately one hour, and enhances the stability of AuNPs against highly ionic solutions. Finally, we also tested a rapid conjugation method known as instant dehydration in butanol (INDEBT) to showcase recent advancements in rapid conjugation techniques.[19] This method rapidly dehydrates DNA and AuNPs in the presence of TCEP and butanol, creating a concentrated environment that reduces electrostatic hindrances and allows for covalent conjugation within 30 minutes (Fig. 1, right).

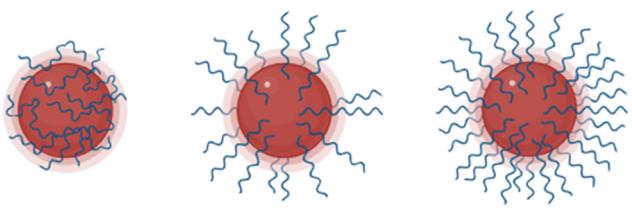

Fig. 1 Schematic illustration of DNA on the surface of AuNPs (left), radial disposition of DNA as a result of SA conjugation protocols (center) and highly concentration of DNA as a result of INDEBT conjugation protocol (right). Created with Biorender.

The storage buffers investigated in this work were 100 mM Tris-$MgCl_2$ (pH 7.4), commonly employed in SELEX processes and recognized for its role in DNA aptamer conformation and polymerase cofactor activity; 10 mM PBS-$MgCl_2$ (pH 7.4), another widely used buffer in biochemical experiments; PBS alone, utilized at various stages of LFA preparation; and deionized water (MQ water), serving to assess storage in the absence of ionic forces and as a control for potential later buffer transitions.[35–38] This systematic assessment is aimed at investigating the impact of different buffers on the stability and performance of DNA–AuNP conjugates.

Each DNA–AuNP conjugate was analysed using electrophoretic mobility shift assays (EMSAs), UV-visible (UV-Vis) spectroscopy, dynamic light scattering (DLS) and Z-potential.[39–41] Furthermore, we assessed the functionality of the conjugates by evaluating their hybridization performance on LFAs with complementary DNA sequences printed onto the nitrocellulose membranes. It is intended that the results herein will aid researchers and manufacturers in choosing the best conju-

gation methods and buffers for their LFAs to make them as stable and robust as possible.

Experimental

Materials

DNA sequences were purchased from LGC Biosearch Technologies. $HAuCl_4$, sodium citrate, Tween-20, polyethylene glycol 2050 (PEG2050), sodium chloride, PBS tablets, trizma salts (Tris), phosphate salts, magnesium chloride, Tris-(2-carboxyethyl)phosphine hydrochloride (TCEP), *n*-butanol, Tris-borate-EDTA (TBE) buffer 10×, glycerol and agarose were purchased from Merck. Transparent 96-well plates were purchased from FisherScientific (Hampton, NH, USA). A SpectraMax iD3 (San José, CA, USA) UV-Vis spectrophotometer was used for absorbance measurements. DLS and Z-potential measurements were performed using DTS1070 cuvettes in a Zetasizer Nano ZS from Malvern Panalytical (U.K.). The electrophoretic system used was a shiroGEL Mini 10, purchased from VWR International, LLC. Lateral flow strips were printed using IsoFlow dispensr (Imagene Technology, USA), scanned using a CanoScan LiDE400 (Canon, Spain), and analyzed using ImageJ software. Lateral flow strips were made of nitrocellulose (CN 150 from Sartorius), cellulose (GE Healthcare), and laminated card (Millipore). Sequences used in this work:

Conjugate sequence: 5′-GGTCGTCCCGAGAGTTTTTTTTTT-TTTT-ThiolC6-3′

Printed sequence: 5′-CTCTCGGGACGACC-biotin-3′

Methods

Conjugate preparation

20 nm AuNPs were synthesized using the Turkevich method and stored at 4 °C before being conjugated on the same day that they were synthesised. The synthesis concentration was determined by UV-Vis measurements to be 1.2 nM (1×). Five conjugation methods were employed, with the starting amounts of AuNPs and DNA normalized and fixed to evaluate each method's effectiveness. The measurements of the AuNP–DNA were started on the same day that the conjugation finished (day 0).

For the SA protocol, 21.2 μL of 100 μM DNA was mixed with 2 μL of 10 mM TCEP and incubated for one hour in the dark with shaking at 600 rpm. Subsequently, 2650 μL of AuNP stock was added and incubated overnight (16 h). The following morning, 330 μL of 1 M NaCl and 330 μL of 0.1 M sodium phosphate buffer (pH 7) were added dropwise while shaking. The solution was incubated for 24 hours, centrifuged at 10 000 rpm for 30 minutes at 10 °C, and resuspended in the required storage buffer to a final volume of 535 μL.

For the SA-pH protocol, 21.2 μL of 100 μM DNA was mixed with 2 μL of 10 mM TCEP and 1 μL of 500 mM Acetate buffer (pH 5.2) and incubated for one hour in the dark with shaking at 600 rpm. Then, 2650 μL of AuNPs was added and incubated overnight (16 h). The following morning, 26.5 μL of 500 mM Tris-acetate buffer (pH 8.2) and 265 μL of 1 M NaCl were added dropwise while shaking. The solution was incubated for 24 hours, centrifuged at 10 000 rpm for 30 minutes at 10 °C, and resuspended in the corresponding storage buffer to a final volume of 535 μL.

For the SA-LF protocol, 21.2 μL of 100 μM DNA was mixed with 2 μL of 10 mM TCEP and incubated for one hour in the dark with shaking at 600 rpm. Then, 2650 μL of AuNPs was added and incubated for another hour. Subsequently, 176.6 μL of 100 mM PBST (1 M NaCl, 0.1% Tween-20) was added dropwise while shaking and incubated for an hour. The solution was sonicated for 10 seconds at moderate intensity, and 88.3 μL of 1 M NaCl were added dropwise while shaking, followed by another hour of incubation. The solution was sonicated again for 10 seconds, followed by the addition of another 88.3 μL of 1 M NaCl, and incubated overnight (16 h). The solution was centrifuged at 10 000 rpm for 30 minutes at 10 °C and resuspended in the corresponding storage buffer to a final volume of 535 μL.

For the polyT-adsorption protocol, 21.2 μL of 100 μM thiolated DNA was added to 2650 μL of AuNPs and incubated for 30 minutes with shaking at 250 rpm. The solution was then centrifuged at 10 000 rpm for 30 minutes at 10 °C and resuspended in the corresponding storage buffer to a final volume of 535 μL.

For the INDEB protocol, 12 mL of AuNPs were centrifuged at 10 000 rpm for 30 minutes at 10 °C and resuspended in 1200 μL of MQ water (10× AuNPs final concentration). For each storage buffer group, 21.2 μL of 100 μM thiolated DNA was mixed with 3 μL of 100 mM TCEP and 265 μL of 10× AuNPs. The mixture was vortexed with 2700 μL of butanol, followed by the addition of 300 μL of 0.5× TBE and another quick vortex. The solution was briefly centrifuged at 2000*g*, the upper butanol layer removed, and the pellet resuspended in the corresponding storage buffer to a final volume of 535 μL.

All conjugates were tested on day 0, 3, 7, 10, 13, 17 and 21, with day 0 being the day that the conjugations were completed. When not used they were stored at 4 °C in the dark.

Characterization methods

EMSAs were performed using a 2% agarose gel. Samples (5 μL) were mixed with 1 μL of 30% glycerol and run for 30 minutes at 120 V (Fig. 2). Gels were photographed and analyzed using ImageJ.

UV-Vis measurements were performed in triplicates at a final concentration of 0.1× using the corresponding storage buffer. Absorbance values were obtained from 400 to 700 nm at 5 nm intervals. DLS and zeta potential measurements were performed using a Malvern Zetasizer Nano ZS at 25 °C. Measurements were taken in triplicates at 0.5× for DLS and 0.125× for the zeta potential LFAs were prepared following a published protocol and the half-stick format.[37] Briefly, sample pads were treated with 0.1% PEG 2050 and 0.05% Tween-20 in 100 mM Tris-$MgCl_2$ buffer and dried overnight at 37 °C. Control lines were printed on the nitrocellulose membrane

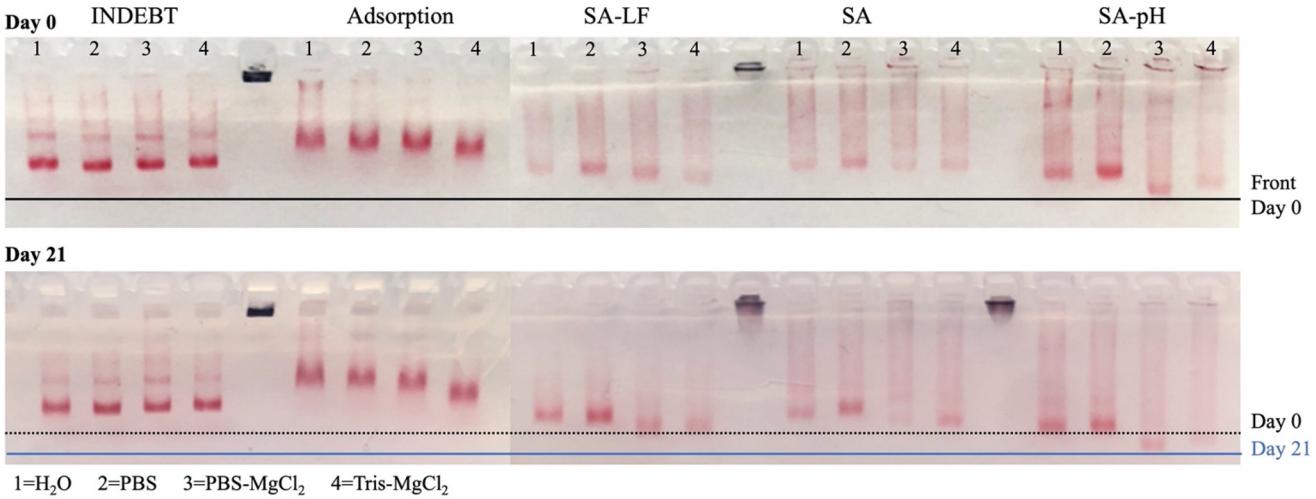

Fig. 2 EMSA results of the 20 conjugates on day 0 (top) and day 21 (bottom). Black lines correspond to the maximum migration distance of the furthest conjugate on day 0 (solid line) and in reference to day 21 migrations (dotted line). The blue line corresponds to the maximum migration distance of the furthest conjugate on day 21. Black deposits in the wells correspond to aggregated AuNPs.

with 40 μM DNA and 10 μM Streptavidin, previously incubated together for 30 minutes. Conjugates were diluted to 0.5× in their respective storage buffers, and 60 μL was added to each sample pad, allowing flow for 15 minutes. Bare AuNPs were diluted in MQ water and tested in the same fashion. Strips were scanned after 20 minutes of running and analysed using ImageJ software, all experiments were performed in triplicate. The LFA strip test lines were printed one day before each testing event and assembled on the testing day.

Results and discussion

Electrophoretic mobility shift assay

The EMSA results on day 0 (Fig. 3, top) indicate that the conjugation method significantly impacts the observed band features, revealing three distinct running fronts associated with polyT-adsorption, INDEBT, and SA conjugation methods (Fig. 2). PolyT-adsorption conjugations display broad and diffuse running fronts and a degree of smearing, suggesting stochastic packing of the nucleobases and resulting in a wide range of conjugation densities and charge states on the AuNPs. This indicates that the polyT-adsorption method achieves the least uniform AuNP coating within a single sample. INDEBT conjugation shows two distinct bands in the EMSA from day 0 in all the storage buffers. Since this phenomenon did not occur with other conjugation methods, it is concluded that INDEBT results in two distinct groups of AuNPs with homogeneous mass-to-charge ratios. This is attributed to the immiscibility of the butanol and water mix used in the method, leading to functionalization in both the aqueous bulk and at the phase interface. SA conjugations exhibit a single band with a solid but less intense running front and a diffuse trail of conjugates. This is attributed to a more heterogeneous population of conjugates with varying amounts of DNA and

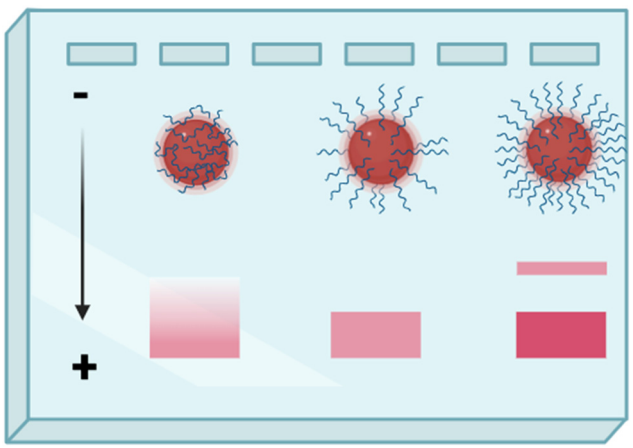

Fig. 3 Schematic representation of the EMSA. Negatively charged DNA–AuNPs flow towards the positive pole of the agarose gel pushed by an electric field. Different densities and disposition of the DNA provokes different mass-to-charge ratios and generate different band morphologies. Created with Biorender.

mass-to-charge ratios. A gradual reduction in size is observed between water, PBS, PBS-$MgCl_2$, and Tris-$MgCl_2$ buffers in polyT-adsorption and SA protocols, a trend which follows the increasing ionic strength of each buffer, so is attributed to electrostatic shielding, which affects the conjugates' pellet resuspension and DNA packing density and secondary structures (Fig. 4, grey). Conversely, INDEBT conjugates are less impacted by the resuspension buffer, likely due to higher packing density and protection of the AuNPs' surface. INDEBT conjugates resuspended in buffers with $MgCl_2$ show a minimal increase in size, suggesting that the DNA conjugated by this method is less prone to rearrangement in different buffers but is slightly susceptible to penetration and rearrangement due to

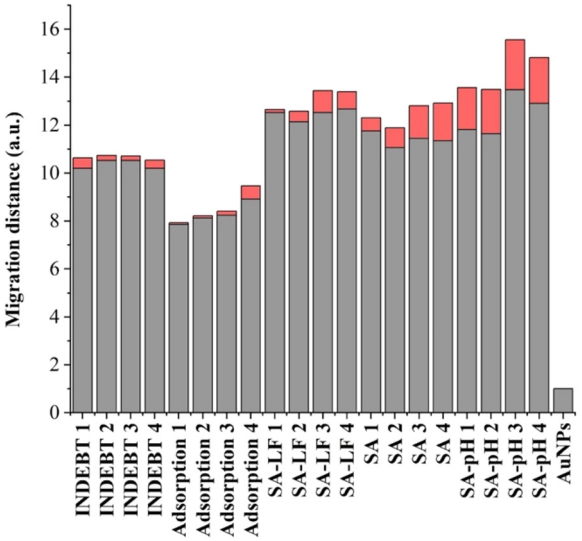

Fig. 4 Migration distances of the conjugates on day 0 (grey) and day 21 (red). With the different storage buffers given as: 1 = water, 2 = PBS, 3 = PBS-$MgCl_2$, 4 = Tris-$MgCl_2$.

Mg^{2+} ions which contribute to ordering DNA more radially. Over time, a general increase in migration distance is observed (Fig. 1, bottom, and Fig. 4, red), suggesting a gradual loss of DNA and reduction in conjugate size/charge. The three SA techniques show a similar initial pattern and tendency over time, with the highest changes in migration distance over 21 days, indicating DNA loss. SA and SA-pH protocols are particularly affected, showing increased migrations in highly ionic buffers and some degree of aggregation, as evidenced by the appearance and disappearance of bands of different sizes (Fig. S1†). SA-LFA conjugation showed no band size changes over three weeks and lower differences in migration distance compared to the other SA techniques.

INDEBT conjugation demonstrates excellent stability over three weeks with no observed changes, in contrast to the other techniques. The EMSA analysis highlights the stability and tolerance of INDEBT conjugation to different storage buffers, making it suitable for long-term assays. Despite the diffuse running front, polyT-adsorption conjugations experience minimal changes in migration, while the three SA methods, particularly SA-pH, are most affected by time and buffer composition. Conjugates stored in water and PBS show smaller changes in migration distances over three weeks, suggesting that increasing ionic strength during storage may be detrimental in the long term. Additionally, non-conjugated AuNPs tend to aggregate when in contact with the TBE buffer, as depicted in Fig. 3. Based on the findings from the EMSA results, INDEBT conjugation offers superior stability and resistance to changes in buffer composition and storage time, making it the most dependable method for long-term assays. In contrast, SA methods, especially SA-pH, show considerable susceptibility to variations in ionic strength and storage conditions, highlighting the importance of carefully selecting conjugation and storage protocols to preserve the integrity of AuNP conjugates.

UV-Vis spectrophotometry

The UV-Vis results (Fig. 5 and S2†) indicate that the three SA processes result in more aggregation than the INDEBT and polyT-adsorption methods, likely due to the salts shielding the citrates of the AuNPs. Maximum absorbance values decreased compared to non-conjugated AuNPs (Fig. S2D and F†), indicating the reduction in the number of nanoparticles due to aggregation, which also resulted in flatter spectra and a decreased 520/580 nm ratio (Fig. 5). Notably, when water resuspensions of the three SA processes from day 0 were examined, higher absorbances and 520/580 nm ratios were observed, suggesting that the final resuspension in highly ionic storage buffers exacerbates the stress from the conjugation process. In contrast, polyT-adsorption and INDEBT protocols maintained values closer to non-conjugated AuNPs, indicating a lower impact on the AuNPs while effectively achieving conjugation and protecting them from additional impact during the resuspension step, in agreement with the EMSA results. An anomaly was noted when water was used to resuspend the polyT-adsorption protocol conjugates (Fig. S2E and S3A†), which resulted in a significant shift of the peak to 550 nm. This is attributed to the low ionic strength of the buffer not shielding neighbouring DNA molecules on the AuNP surface, increasing electrostatic stress within the layer, causing it to break apart and leading to bare Au and therefore aggregation. Among the storage buffers, PBS exhibited behaviour most similar to water resuspensions, maintaining a low aggregation ratio while avoiding the significant shift seen in the aqueous polyT-adsorption conjugate (Fig. S3B†).

PBS-$MgCl_2$ and Tris-$MgCl_2$ buffers affected the conjugates differently, showing the lowest absorbances and increased flattening of the spectra since day 0, particularly in the three SA conjugations. The polyT-adsorption and INDEBT protocols experienced less aggregation in these buffers than the SA conjugates.

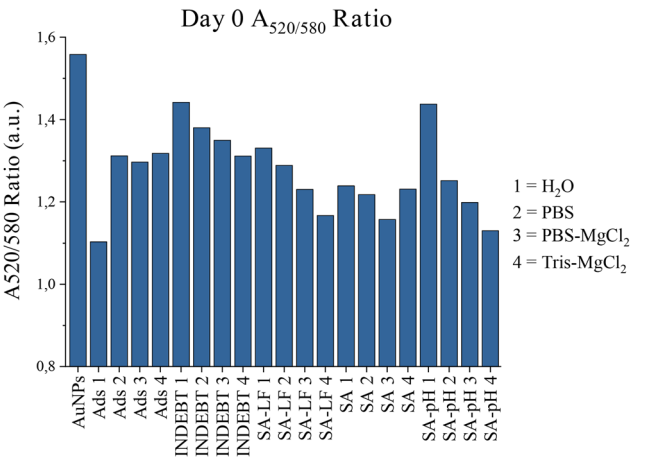

Fig. 5 $A_{520/580}$ ratio of all conjugates and non-conjugated AuNPs on day 0.

Table 1 Average of the 21 days of the conjugates and non-conjugated AuNPs' *Z*-averages. All values are in nm

	SA	SA-pH	SA-LF	INDEBT	Adsorption
Water	61.59 ± 16.19	43.99 ± 7.52	56.35 ± 13.72	63.90 ± 13.45	52.39 ± 6.5
PBS	63.71 ± 24.45	41.81 ± 11.84	58.51 ± 18.71	65.87 ± 17.85	62.11 ± 13.90
PBS-$MgCl_2$	87.24 ± 16.96	70.23 ± 19.40	106.63 ± 57.46	93.2 ± 33.75	106.64 ± 63.70
Tris-$MgCl_2$	136.03 ± 106.44	127.78 ± 80.80	111.82 ± 104.58	83.175 ± 66.81	66.85 ± 44.36
AuNPs	40.05 ± 11.72				

During the three-weeks tested, water resuspensions were consistently more stable and had better aggregation ratios than PBS or PBS-$MgCl_2$ (Fig. S4B†). Water resuspensions showed higher and constant absorbance values over 21 days, whereas PBS and PBS-$MgCl_2$ conjugates exhibited more variability over the same period. By day 21, Tris-$MgCl_2$ conjugates exhibited visible aggregation.

UV-Vis measurements effectively monitored aggregation over 21 days, revealing two types of aggregation events: during the conjugation steps and during the resuspension of the centrifuged pellet. The stability of the AuNP–DNA was partially compromised during the three SA processes, while polyT-adsorption and INDEBT protocols did not show this effect. Furthermore, the aggregation during resuspension was significantly influenced by the ionic strength of the buffers. INDEBT and polyT-adsorption conjugates were less affected by resuspension in highly ionic buffers, maintaining stability over time. This suggests that these methods effectively conjugate and protect AuNPs, reducing AuNP or DNA loss and providing further protection against reconcentration or dilution. Resuspended conjugates in water or PBS generally remained stable over 21 days, regardless of the conjugation process used. However, $MgCl_2$-containing buffers, especially Tris-$MgCl_2$, did not provide a favourable environment for long-term storage of DNA–AuNP conjugates. It is proposed that the presence of the divalent Mg^{2+} ions results in a change in the secondary structure of the DNA, through its coordination with the phosphate backbone of the DNA strands, which results in increased stress and instability of the films, which leads to rearrangement or loss of DNA and exposed Au, which causes aggregation.

DLS and Z-potential measurements

Throughout the 21-day investigation, DLS measurements were performed to analyse the conjugates.

The DLS results can be analysed in various ways, but for this work the mean hydrodynamic diameter of the nanoparticles "*z*-average" and the polydispersity index (PdI) will be analyzed. The PdI is a measure of the distribution of sizes within the sample, the lower the value being more indicative of a monodispersed suspension. The PdI of the different conjugates in each of the buffers, over 21 days, is provided in Fig. S5.† In this data we can see that all the PdI are within the accepted range for nanoparticles of this size, 0.2–0.5 a.u. There are also a couple of trends observable in this data, notably that the unconjugated AuNPs become less evenly dispersed from day 10 in every storage buffer, the INDEBT conjugation produces the most stable and well dispersed conjugates, and that the Tris-$MgCl_2$ buffer is the worst in terms of variability and polydispersity. The hydrodynamic diameter of the conjugates over time in different buffers is provided in Table 1 and Fig. S6.† In this data we can see that the conjugates are the same size (30–100 nm) within experimental error in water and PBS. The data also shows that the particle sizes do not change over the three weeks investigated. There is perhaps a trend in this data of the bare AuNPs being smaller than the other conjugates, as would be expected, but this is not significant or conclusive by these measurements alone. Although it is worth noting as they are not affected by the trends in the Mg^{2+} containing buffers, like the other conjugates. The PBS-$MgCl_2$ and Tris-$MgCl_2$ buffers give *Z*-averages that are larger than in the water and PBS, showing more variation and irreproducibility, with spikes in diameter over time. There is also a noticeable increase in diameter between days 17 and 21 in the Tris-$MgCl_2$, which is attributed to aggregation. These buffers causing issues is suggestive of the Mg^{2+} ions disrupting the AuNP–DNA conjugates, most probably by changing the secondary structure of the DNA through ionic interactions with the phosphate backbone. This is in agreement with the other techniques used in this study and suggests that DNA conjugates are susceptible to interference from divalent ions such as Mg^{2+}.

Lateral flow assay tests

LFA analysis was performed to assess the functionality of the DNA–AuNP conjugates. After flowing, the strips were scanned, and the intensity of the test lines measured using "Image J". The signal intensities were categorized into three distinct outcomes: signals with intensities ranging from 0 to approximately 15 units indicated no detectable signal, since these results could be found in blank samples. Intensities of 15 to 50 units represented weak positive signals, while intensities greater than 50 units were labelled strong positives. Non-functionalized AuNPs, employed as negative controls, consistently exhibited aggregation, and therefore could not flow properly through the nitrocellulose in any buffer from day 0 onwards (Fig. 6). The levels of non-specific adsorption of functionalised nanoparticles to the nitrocellulose could be determined from those conjugates where no signal was observed. In some samples where the streptavidin was printed, no line could be observed, showing that non-specific adsorption was not a significant factor in these experiments.

The results of these tests on day 0 show that the LFA performance is not as dependent on the conjugation method as it

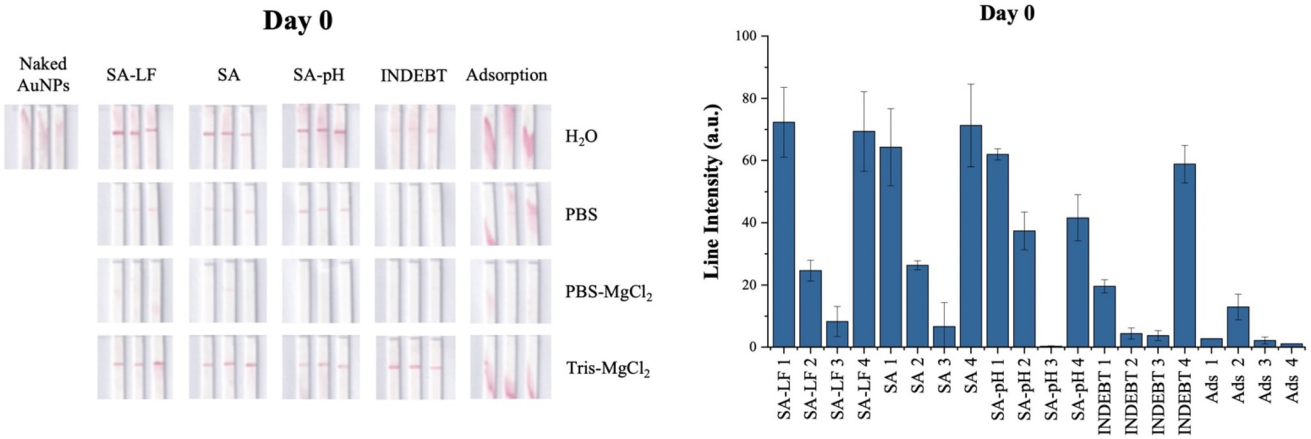

Fig. 6 Lateral flow results of day 0. Left, lateral flow strips. Right, ImageJ quantification. 1 = water, 2 = PBS, 3 = PBS-$MgCl_2$, 4 = Tris-$MgCl_2$.

is on the buffer, with the notable exception of the polyT-adsorption protocol which was not functional in any of the buffers investigated. The SA and INDEBT conjugations were all most functional in MQ water and Tris-$MgCl_2$, with the SA performing generally better in the water and the INDEBT better in the Tris. The poorer performances of all the conjugates in the phosphate containing buffers may indicate that the presence of the phosphate ions may be hindering the LFA performance.

These tests were repeated after 21 days of storing the conjugates in the different buffers, Fig. 7. The LFA performance of all the conjugates in all the buffers was seen to significantly decrease. Most notably the INDEBT conjugates in Tris became non-functional. The hydrodynamic diameter and electrophoretic mobility of these conjugates are stable over the three weeks investigated, and the samples did not aggregate. We hypothesise that this data is evidence of the presence of residual butanol on the nanoparticle conjugates. The partition coefficient of Tris from water into alcohol solvents is known to be complex, varying with solvent composition, which we believe will change over the timescale measured herein as the butanol evaporates.[42] This causes large scale reordering of the water molecules at the conjugate solution interface over time, may explain the difference in performance over time in the Tris buffer and INDEBT conjugates. These data emphasize the importance of solvation in the functionality and performance of the conjugates.

During the stability studies, the SA-LFA protocol exhibited the most rapid decay in signal intensity, particularly noticeable from day 3 onwards (Fig. S7†). The SA-pH protocol maintained stable signals until day 10 for water and PBS but declined by day 21 (Fig. S8†). The SA protocol also sustained stable signals until day 14, with water resuspensions showing a linear decrease in signal intensity (Fig. S9†). These data would suggest that all SA conjugations will suffer from some loss of functionality over a few weeks, regardless of the storage buffer, but that they are, in general superior to the other conjugation methods tested.

Conjugate comparisons

The EMSA, UV-Vis spectroscopy, DLS measurements, and LFAs provided a comprehensive assessment of DNA–AuNP conjugates' characteristics, stability, and functionality over a 21-day

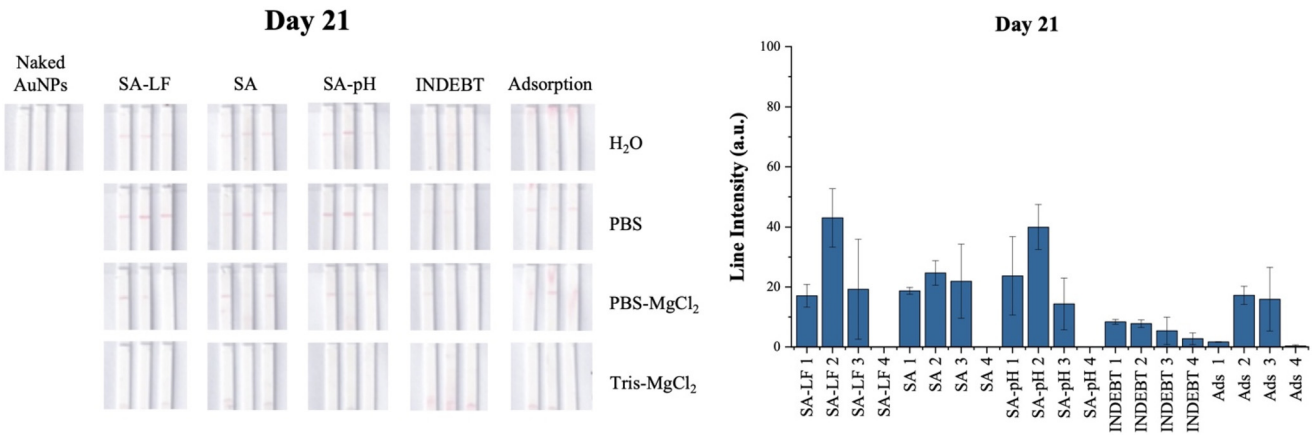

Fig. 7 Lateral flow results of day 21. Left, lateral flow strips. Right, ImageJ quantification. 1 = water, 2 = PBS, 3 = PBS-$MgCl_2$, 4 = Tris-$MgCl_2$.

period. These techniques collectively offered complementary insights into size distribution, packing density and structure of the nucleic acids, as well as the aggregation states of the AuNP–DNA conjugates. In evaluating the functionality of DNA–AuNP conjugates in LFA over 21 days, distinct groups emerged based on their performance and characteristics. Firstly, polyT-adsorption conjugates were consistently non-functional despite maintaining stable absorbance ratios, *Z*-averages, and EMSA migration distances, indicating low levels of aggregation.

All conjugates that were initially functional in LFAs showed declining performance over time. None more than INDEBT conjugates which showed two distinct EMSA populations, and suffered irregular LFA functionality possibly due to butanol residues hindering flow and hybridization. Despite this, their stability suggests potential use in compatible applications.

In contrast, six conjugates, primarily the SA methods with water or PBS buffers, maintained functionality until day 21. SA techniques demonstrated compatibility with LFA, with SA and SA-pH methods showing similar functionality levels. LFA-optimized SA protocols initially performed well but deteriorated faster, suggesting limitations for long-term use.

Buffer comparisons

The selection of resuspension buffers played a critical role in maintaining conjugate stability. Conjugates stored in Mg^{2+}-free, low-ionic strength buffers such as deionized water and PBS exhibited enhanced long-term stability and reduced aggregation. In contrast, buffers containing Mg^{2+} cations promoted aggregation and decreased functionality over time.

Conjugates resuspended in PBS-$MgCl_2$ were consistently non-functional in LFAs, showed increased migration in EMSA, more aggregation, and irregular absorbance and hydrodynamic profiles. There is a trend of phosphate containing buffers, PBS and PBS-$MgCl_2$, not being functional in LFA with any of the conjugates, implying that the phosphate, or some other component specific to these buffers, is somehow impairing DNA conjugate hybridization to the test line DNA. The exact methodology of this is not known as it does not fit with any of the other observations. All that can be said is that the explanation should comply with changes that do not show in DLS, Z-potential, UV/Vis or EMSA changes in the conjugates, and should apply to all the conjugation chemistries tested. All conjugates that were initially functional in LFAs showed declining performance over time, however, none more than those resuspended in Tris-$MgCl_2$. Conjugates resuspended in Tris-$MgCl_2$ initially performed well in LFA but degraded by day 14 with aggregation visible to the naked eye, corroborated with changes in EMSA and UV-Vis metrics.

Water resuspensions consistently supported LFA functionality, corroborated by EMSA, UV-Vis, and DLS measurements.

This study underscores the critical role of buffer compatibility and optimization conditions in LFA performance, providing insights into maintaining stability and functionality of DNA–AuNP conjugates across varied applications.

Conclusions

The integrated use of EMSA, UV-Vis spectroscopy, and DLS provided complementary insights into DNA–AuNP conjugate state, stability, and functionality. This multi-faceted approach was essential for capturing nuanced changes within the conjugate samples, enhancing understanding beyond what could be discerned from LFA functionality alone.

The choice of conjugation method significantly influenced nucleic acid density and functionality on AuNP surfaces, impacting their protection against aggregation and overall stability. SA and SA-pH methods demonstrated higher compatibility and stability in LFAs, contrasting with the INDEBT method which, despite initially working in Tris buffer, failed over time due to residual butanol and Tris interactions hindering hybridization processes. Future work will investigate if more stringent removal of butanol can overcome this issue.

PolyT-adsorption conjugates and those stored in phosphate containing buffers consistently failed in LFAs. Indicating that the phosphate ions may be inhibiting correct DNA-LFA function. This is an important consideration as phosphate containing buffers are routinely used in conventional antibody based LFAs, and in aptameric sensors, which may encounter problems when being transferred into a LFA format.

Practical recommendations derived from this study include the preferential use of SA-LF for immediate applications and the SA-pH method in phosphate and Mg^{2+}-free buffers for longer storage periods. Moreover, careful consideration of resuspension buffer composition and LFA treatment conditions is crucial to maintaining sensitivity and ensuring optimal performance.

Author contributions

Conceptualization, C. P., A. P.; formal analysis, C. F. C., A. P., and C. P.; investigation, C. F. C., A. P.; methodology, C. F. C.; supervision, C. P., A. P. and A. M.; validation, C. F. C., C. P. and A. P.; visualization, C. F. C.; writing – original draft, C. F. C., writing – review & editing, all authors. All authors have read and agreed to the published version of the manuscript.

Data availability

The data supporting this article have been included as part of the ESI.†

Conflicts of interest

There are no conflicts to declare.

Acknowledgements

The MICROB-PREDICT project has received funding from the European Union's Horizon 2020 Research & Innovation Program under grant agreement no. 825694. This article reflects only the authors' view, and the European Commission is not responsible for any use that may be made of the information contained therein. This work was also part funded by the FULLPOC project; AEI Plan Nacional; Grant PID2021-124795NB-I00 funded by MCIN/AEI/ 10.13039/501100011033. at the Catalan Institute of Nanoscience and Nanotechnology (ICN2); The ISGlobal author acknowledges support from the Spanish Ministry of Science and Innovation and State Research Agency through the "Centro de Excelencia Severo Ochoa 2019–2023" Program (CEX2018-000806-S). C.P. acknowledges support from the Spanish Ministry of Science through the Ramón y Cajal grant no. RYC2022-036743-I.

References

1 J. I. Cutler, E. Auyeung and C. A. Mirkin, *Spherical Nucleic Acids*, 2021, **1**, 91–136.
2 M. Li, Y. C. Lin, C. C. Wu and H. S. Liu, *Nucleic Acids Res.*, 2005, **33**, e184.
3 J. Sun, A. Guo, Z. Zhang, L. Guo and J. Xie, *Sensors*, 2011, **11**, 10490–10501.
4 S. Dalirirad and A. J. Steckl, *Anal. Biochem*, 2020, **596**, 113637.
5 L. Meng, W. Ma, S. Lin, S. Shi, Y. Li and Y. Lin, *ACS Appl. Mater. Interfaces*, 2019, **11**, 6850–6857.
6 J. L. Gao, Y. H. Liu, B. Zheng, J. X. Liu, W. K. Fang, D. Liu, X. M. Sun, H. W. Tang and C. Y. Li, *ACS Appl. Mater. Interfaces*, 2021, **13**, 31485–31494.
7 S. Y. Park, A. K. R. Lytton-Jean, B. Lee, S. Weigand, G. C. Schatz and C. A. Mirkin, *Nature*, 2008, **451**, 553–556.
8 W. Page Faulk and G. Malcolm Taylor, *Immunochemistry*, 1971, **8**, 1081–1083.
9 S. K. Vashist and J. H. T. Luong, Chapter 17 – Immunoassays: Future Prospects and Possibilities, In Handbook of Immunoassay Technologies, 2018, pp. 455–466.
10 K. J. Land, D. I. Boeras, X. S. Chen, A. R. Ramsay and R. W. Peeling, *Nat. Microbiol.*, 2019, **4**, 46–54.
11 B. G. Andryukov, *AIMS Microbiol.*, 2020, **6**, 280.
12 C. A. Mirkin, R. L. Letsinger, R. C. Mucic and J. J. Storhoff, *Spherical Nucleic Acids*, 2021, **1**, 3–11.
13 B. Liu and J. Liu, *Anal. Methods*, 2017, **9**, 2633–2643.
14 Q. Ding, W. Qiu, C. Sun, H. Ren and G. Liu, *Molecules*, 2023, **28**, 4480.
15 W. Zhao, L. Lin and I. M. Hsing, *Bioconjugate Chem.*, 2009, **20**, 1218–1222.
16 T. A. Taton, *Curr. Protoc. Nucleic Acid Chem.*, 2002, **9**, 1–12.
17 B. Liu and J. Liu, *Anal. Methods*, 2017, **9**, 2633–2643.
18 B. Liu and J. Liu, *J. Am. Chem. Soc.*, 2017, **139**, 9471–9474.
19 Z. Huang and J. Liu, *Matter*, 2021, **4**, 2585–2586.
20 J. Liu and Y. Lu, *Angew. Chem., Int. Ed.*, 2005, **45**, 90–94.
21 M. Huang, E. Xiong, Y. Wang, M. Hu, H. Yue, T. Tian, D. Zhu, H. Liu and X. Zhou, *Nat. Commun.*, 2022, **13**(968), 1–14.
22 A. Chen and S. Yang, *Biosens. Bioelectron.*, 2015, **71**, 230–242.
23 W. N. Fang, C. H. Fan and H. J. Liu, *Acta Polym. Sin.*, 2017, 1993–2000.
24 N. Bhatt, P. J. J. Huang, N. Dave and J. Liu, *Langmuir*, 2011, **27**, 6132–6137.
25 S. Sangwan and R. Seth, *J. Cluster Sci.*, 2022, **33**, 749–764.
26 A. J. H. Hoa and T. Phan, *Physiol. Behav.*, 2017, **176**, 100–106.
27 S. J. H. Hurst, A. K. R. L-J Lytton-Jean and C. A. M. Mirkin, *Anal. Chem.*, 2006, **78**(24), 8313–8318.
28 M. Cárdenas, J. Barauskas, K. Schullén, J. L. Brennan, M. Brust and T. Nylander, *Langmuir*, 2006, **22**, 3294–3299.
29 J. Christopher Love, A. Lara, K. Jennah, G. Ralph and M. George, *Chem. Rev.*, 2005, **105**, 1103–1170.
30 C. A. Mirkin and G. B. Rathmann, *MRS Bull.*, 2010, **35**, 532–539.
31 D. S. Seferos, A. E. Prigodich, D. A. Giljohann, P. C. Patel and C. A. Mirkin, *Spherical Nucleic Acids*, 2021, **1**, 425–435.
32 A. P. Alivisatos, K. P. Johnsson, X. Peng, T. E. Wilson, C. J. Loweth, M. P. Bruchez and P. G. Schultz, *Nature*, 1996, **382**, 609–611.
33 J. Liu and Y. Lu, *Nat. Protoc.*, 2006, **1**, 246–252.
34 X. Zhang, M. R. Servos and J. Liu, *Langmuir*, 2012, **28**, 3896–3902.
35 A. H. Buck, C. J. Campbell, P. Dickinson, C. P. Mountford, H. C. Stoquert, J. G. Terry, S. A. G. Evans, L. M. Keane, T. J. Su, A. R. Mount, A. J. Walton, J. S. Beattie, J. Crain and P. Ghazal, *Anal. Chem.*, 2007, **79**, 4724–4728.
36 Y. S. Kim, C. J. Hyun, I. A. Kim and M. B. Gu, *Bioorg. Med. Chem.*, 2010, **18**, 3467–3473.
37 C. Parolo, A. Sena-Torralba, J. F. J. F. Bergua, E. Calucho, C. Fuentes-Chust, L. Hu, L. Rivas, R. Álvarez-Diduk, E. Nguyen, S. Cinti, D. Quesada-González and A. Merkoçi, *Nat. Protoc.*, 2020, **15**, 3788–3816.
38 N. Komarova and A. Kuznetsov, *Molecules*, 2019, **24**, 3598.
39 S. Bhattacharjee, *J. Controlled Release*, 2016, **235**, 337–351.
40 J. M. Walker, *Biosensors*, 2009, **504**, 399–415.
41 P. Englebienne, A. Van Hoonacker and M. Verhas, *Spectroscopy*, 2012, **17**, 255–273.
42 P. Schindler, R. A. Robinson and R. G. Bates, *J. Res. Natl. Bur. Stand., Sect. A*, 1968, **72**, 141.